1

Automated Rovibrational Configuration Interaction Calculations

Subhasish DAS and Guntram RAUHUT
University of Stuttgart, Germany

1.1. Introduction

The calculation of rovibrational infrared spectra of molecules without the use of model Hamiltonians is a demanding task, which includes several computational bottlenecks and requires the monitoring of intermediate quantities. These comprise, for example, the generation of a multidimensional potential energy surface (PES), the calculation of tightly converged vibrational wavefunctions, which serve as basis functions in the subsequent rovibrational configuration interaction (RVCI) calculation and so on. If all these parts of the calculation were fast, it would be easy to automate these calculations, but unfortunately this is not the case. In order to limit the computational effort, commonly series expansions are introduced, which need to be checked for convergence. Usually, a number of parameters and thresholds go along with such implementations, which are needed to properly control the respective calculations. However, an inexperienced user typically has some problems to handle such a software package as the technical details require a deep theoretical understanding, which often limits the use of such programs to experts. This is an unfortunate situation and thus the program should control itself by error recognition and correction schemes and by the automated calculation of some program parameters as, for example, the number of vibrational basis functions, the maximal

High-Resolution Molecular Spectroscopy 1B,
coordinated by Iwona GULACZYK, Michaël REY and Ha TRAN.

rotational quantum number, any symmetry information or the nuclear spin statistical weights. In this chapter, we outline the computational workflow of an implementation of RVCI theory in the MOLPRO package of ab initio programs (Werner et al. 2020), which requires just a bare minimum of information from the user to generate a high-quality spectrum, which pops out at the end. The main information to be provided by the user concerns an approximate molecular structure and the level of theory to be used for calculating the PES. This allows for routine calculations even in practical classes at the undergraduate level and the focus could thus be shifted from the quantum chemical calculation to the interpretation of the resulting spectra. This is highly desirable as the recent progress in astrophysics and the hunt for new molecules in the interstellar medium or in protoplanetary disks requires the calculation of rovibrational spectra for a multitude of molecules, which often are difficult to synthesize in a lab.

1.2. The Hamiltonian

The simplest exact rovibrational Hamiltonian for polyatomic molecules is that of Watson (1968) (see equation [1.1]). However, it is bound to rectilinear normal coordinates $\mathbf{q}$ or any linear combinations of these. In the following, we will exclusively focus on this Hamiltonian, although attractive alternatives as, for example, the Podolsky Hamiltonian (Podolsky 1928) or the Hougen–Bunker–Johns Hamiltonian (Hougen et al. 1970) do exist.

$$H = \underbrace{\frac{1}{2}\sum_{\alpha\beta} J_\alpha \mu_{\alpha\beta} J_\beta}_{H_{\text{rot}}} - \underbrace{\frac{1}{2}\sum_{\alpha\beta}(J_\alpha \mu_{\alpha\beta}\pi_\beta + \pi_\alpha \mu_{\alpha\beta} J_\beta)}_{H_{\text{cor}}}$$
$$+ \underbrace{\frac{1}{2}\sum_{\alpha\beta}\pi_\alpha \mu_{\alpha\beta}\pi_\beta - \frac{1}{2}\sum_i \frac{\partial^2}{\partial q_i^2} - \frac{1}{8}\sum_\alpha \mu_{\alpha\alpha} + V(\mathbf{q})}_{H_{\text{vib}}} \qquad [1.1]$$

π_α denotes the vibrational angular momentum operator (Watson 1968) for the Cartesian component α:

$$\pi_\alpha = -i \sum_{ij}^{3N-6} \zeta_{ij}^\alpha q_i \frac{\partial}{\partial q_j}, \qquad [1.2]$$

with $\boldsymbol{\zeta}^\alpha$ being the antisymmetric matrix of the Coriolis ζ-constants. Within the Watson Hamiltonian, the $\boldsymbol{\mu}$-tensor, which is the inverse of an effective moment of inertia tensor $\mathbf{I}'$, is given as:

$$\boldsymbol{\mu}(\mathbf{q}) = (\mathbf{I}')^{-1} \qquad \text{with} \qquad I'_{\alpha\beta} = I_{\alpha\beta} - \sum_{ijk} \zeta_{ij}^\alpha \zeta_{kj}^\beta q_i q_k \qquad [1.3]$$

and is usually expanded in some kind of series. Our implementation is based on an n-mode expansion (Bowman et al. 2008), which is also used for the PES, $V(\mathbf{q})$, and the dipole moment surface (DMS), that is:

$$\mu_{\alpha\beta}(\mathbf{q}) = \mu^{(0)}_{\alpha\beta} + \sum_i \sum_r \mu^{(1),r}_{\alpha\beta,i} q_i^r + \sum_{i<j} \sum_{rs} \mu^{(2),rs}_{\alpha\beta,ij} q_i^r q_j^s + ... \quad [1.4]$$

The expansion coefficients, $\boldsymbol{\mu}^{(0)}, \boldsymbol{\mu}^{(1)}, ...$, can be obtained from any fitting procedure, but we rely exclusively on Kronecker product fitting (Ziegler and Rauhut 2016), which was found to be very fast and memory efficient. Clearly, this expansion enters into most terms of the Watson Hamiltonian and thus the convergence of the individual terms, for example, H_{rot} or H_{cor} must be controlled (Tschöpe and Rauhut 2022). While the evaluation of the $\boldsymbol{\mu}$-tensor elements itself is straightforward and fast, the corresponding determination of the Hamiltonian contributions may not. Note that, due to the n-mode expansion, the Coriolis term of equation [1.1] cannot be simplified, because the vibrational angular momentum operator does not commute with respect to the individual $\boldsymbol{\mu}$-tensor terms (see below). The Watson correction term, that is, $-\frac{1}{8}\sum_\alpha \mu_{\alpha\alpha}$, is commonly converged after the third-order contributions and is added as a mass-dependent pseudopotential to the PES expansion.

The PES itself can be generated in a fully automated manner (Schneider et al. 2023), but of course the computational costs may be substantial once high accuracy is needed. It is the combination of several techniques and approximations, which renders its computation feasible for systems of up to 20 atoms (Oschetzki and Rauhut 2014). These can be grouped into techniques, which aim at a reduction of the number of grid points for representing the PES and those, which focus on diminishing the computational cost for an individual electronic structure calculation. Moreover, as the grid point calculations are usually independent from each other, significant speedups can be obtained from embarrassing parallelizations. The most important aspects concerning the acceleration of the PES determination are (a) the twofold exploitation of symmetry, that is, within the electronic structure calculations and within the individual terms of the PES expansion, (b) an intermediate fitting of the grid points to analytical functions, (c) (pre)screening techniques and (d) the use of multi-level techniques within the PES expansion (Rauhut 2004). The latter approach (Pflüger et al. 2005; Sparta et al. 2009) makes use of the fact that the importance of high-order coupling terms within the n-mode expansion of the PES decreases and can thus efficiently be approximated by electronic structure methods of lower accuracy. Once the different levels of theory are properly chosen, the introduced error in the final fundamental frequencies is often in the (sub)wavenumber regime. On the other hand, the computational savings are tremendous. An example is given for oxirane, C_2H_4O, in Table 1.1. The timings in this table refer to a calculation on 48 cores on a customary workstation. Note that the calculation of the 1D potentials took longer than the determination of the harmonic frequencies, despite the smaller number of

grid points, because calculations at the other electronic structure levels are also needed for the evaluation of the 2D to 4D terms. This multi-level scheme led to a mean absolute deviation (MAD) of 2.3 cm^{-1} (see below) with respect to experimental gas phase data for the fundamental vibrations and is thus in the regime of the intrinsic coupled-cluster accuracy (Rauhut et al. 2009) and Ne matrix isolation measurements (Strom et al. 2024). In total, the determination of the PES took about 19 h, while the CPU time for a corresponding calculation without a multi-level scheme can be estimated to last about 21 days. Apparently, the PES expansion has been truncated after the four-mode coupling terms of the n-mode expansion. It has been shown recently that these terms need to be included once the PES is spanned in terms of normal coordinates and once high accuracy is required (Schröder and Rauhut 2024). Clearly, this level of accuracy is not sufficient for a quantitative assignment of individual rovibrational transitions, but for a qualitative interpretation of the spectrum. Further refinements would require the explicit consideration of high-order coupled-cluster terms, relativistic contributions, core correlation effects, non-adiabatic correction terms and so on (Schröder 2023; Koput 2019). Likewise, experimental information can be used to refine such PESs (Mant et al. 2018; Nikitin et al. 2014). With respect to CPU times, the use of explicitly correlated methods is particularly appealing as the cardinal number of the basis set can be reduced by 2 without losing accuracy (Knizia et al. 2009). Likewise, the distinguishable clusters approximation (DCSD) is very attractive, because the triple excitations can be omitted while retaining very high accuracy (Kats and Manby 2013). It can also be seen from Table 1.1 that four-mode couplings can be afforded despite the large number of grid points, because of the much lower computational cost for the MP2 calculations. The bottleneck appears to be the calculation of the 3D terms. Consequently, there are hardly any arguments to neglect the calculation of the four-mode coupling terms within the calculations of accurate PESs.

Calc.	Method	Basis set	Grid points	CPU (min.)
Harm.	CCSD(T)-F12b	cc-pVTZ-F12	129	32
1D	CCSD(T)-F12b	cc-pVTZ-F12	80	54
2D	DCSD-F12b	cc-pVTZ-F12	2,186	252
3D	DCSD-F12b	cc-pVDZ-F12	33,236	655
4D	MP2	cc-pVDZ	179,573	147

Table 1.1. *A multi-level PES of oxirane*

Once the PES has been generated in terms of grid points, it can be converted into an analytical representation by Kronecker product fitting (Ziegler and Rauhut 2016) with hardly any loss in accuracy. The type of the fitting functions is determined automatically by cross-validation and the current library comprises polynomials, B-splines, Gaussians, Morse functions or trigonometric functions (Schneider and Rauhut 2024). Likewise, the number of fitting functions is also determined

automatically by a least-squares criterion. Note that this transformation generates a sum-of-products (SOP) form of the PES, which later on avoids the calculation of any multidimensional integrals.

1.3. VSCF/VCI calculations

As soon as the Hamiltonian has been set up, one would in principle be in the position to solve the rovibrational problem variationally in a finite basis representation by, for example, employing a basis of harmonic oscillator (HO) functions. However, this would lead to huge RVCI matrices, which would render the associated diagonalizations essentially unfeasible. Therefore, basis optimizations are crucial, which can be accomplished by vibrational self-consistent field (VSCF) and vibrational configuration interaction (VCI) calculations for $J = 0$. VSCF theory aims at an optimization of the one-mode wavefunctions (modals), φ_i^I, belonging to a Hartree product (configuration) I, which in turn describes the multidimensional wavefunction (Carney et al. 1978; Bowman 1978):

$$\Psi^I = \prod_i \varphi_i^I(q_i) \qquad \text{with} \qquad \varphi_i^I = \sum_\mu C_{\mu i}^I \chi_{\mu i} \tag{1.5}$$

$\chi_{\mu i}$ are mode-specific basis functions, for example, HO functions, distributed Gaussians or B-splines, and their coefficients $C_{\mu i}^I$ need to be optimized within the VSCF iterations. Once the PES is represented by the analytical functions $b_{ir}(q_i)$, which depend on just one coordinate, it is convenient to introduce the integrals:

$$T_{\mu\nu}^i = \left\langle \chi_{\mu i} \left| \frac{\partial^2}{\partial q_i^2} \right| \chi_{\nu i} \right\rangle \qquad Q_{\mu\nu}^{ir} = \langle \chi_{\mu i} | b_{ir}(q_i) | \chi_{\nu i} \rangle \tag{1.6}$$

$$\tilde{Q}_{ir}^I = \sum_{\mu\nu} C_{\mu i}^I C_{\nu i}^I Q_{\mu\nu}^{ir} \tag{1.7}$$

Neglecting the vibrational angular momentum terms in H_{vib} (see equation [1.1]), the expectation value of the energy can be expressed as:

$$E_I = \sum_i \sum_{\mu\nu} C_{\mu i}^I C_{\nu i}^I \left[-\frac{1}{2} T_{\mu\nu}^i + \sum_r Q_{\mu\nu}^{ir} \left[p_i^{(1),r} + \sum_j \sum_s \tilde{Q}_{js}^I \left[\frac{1}{2} p_{ij}^{(2),rs} + \dots \right] \right] \right] \tag{1.8}$$

$\mathbf{p}^{(1)}, \mathbf{p}^{(2)}, \ldots$ denote the coefficients associated with the basis functions b_{ir} of the PES expansion. Requesting normality of the modals yields the Lagrangian:

$$L = E_I - \sum_i \varepsilon_i^I \left(\langle \varphi_i^I | \varphi_i^I \rangle - 1 \right) \qquad [1.9]$$

Variation of the Lagrangian with respect to the modal coefficients $\mathbf{C}$ finally leads to a mode-specific Fock-type matrix:

$$F_{\mu\nu}^{i,I} = -\frac{1}{2} T_{\mu\nu}^i + \sum_r Q_{\mu\nu}^{ir} \bar{p}_{ir}^I \qquad [1.10]$$

in the primitive basis, where $\bar{p}_{ir}^I$ denotes the effective one-dimensional potential function given by:

$$\bar{p}_{ir}^I = p_r^{(1),r} + \sum_j \sum_s \tilde{Q}_{js}^I \left[p_{ij}^{(2),rs} + \sum_k \sum_t \left[\frac{1}{2} p_{ijk}^{(3),rst} + \ldots \right] \right] \qquad [1.11]$$

As the Fock-type matrix $\mathbf{F}$, which enters into a (generalized) eigenvalue equation for determining the modal coefficients $\mathbf{C}$, depends on these itself, the equations must be solved iteratively until self-consistency has been obtained. The initial guess of this procedure can be generated by neglecting any mode couplings in the representation of the PES, resulting in a one-dimensional Schrödinger equation. Of course, once an orthonormal HO basis has been employed, the generalized eigenvalue problem reduces to a standard one. Typically, not more than 10 VSCF iterations are needed to obtain well-converged results, but if necessary this number can be reduced by direct inversion of the iterative subspace (DIIS) techniques (Yang et al. 2023). The inclusion of vibrational angular momentum terms within the approximation of a constant $\boldsymbol{\mu}$-tensor leads to a correction term $G_{\mu\nu}^{i,I}$ to be added to the Fock-like matrix, which has the form:

$$\begin{aligned} G_{\mu\nu}^{i,I} = & -\frac{1}{2} \sum_{\alpha\beta} \mu_{\alpha\beta}^{(0)} \sum_j \zeta_{ij}^\alpha \zeta_{ij}^\beta \left[T_{\mu\nu}^i \left(\tilde{Q}_{j2}^I - \tilde{Q}_{j1}^I \tilde{Q}_{j1}^I \right) + \tilde{T}_j^I \left(Q_{\mu\nu}^{i2} - 2 Q_{\mu\nu}^{i1} \tilde{Q}_{i1}^I \right) \right] \\ & -\frac{1}{2} \sum_{\alpha\beta} \mu_{\alpha\beta}^{(0)} \sum_{jk} \zeta_{ij}^\alpha \left[2 \zeta_{kj}^\beta \tilde{T}_j^I Q_{\mu\nu}^{i1} \tilde{Q}_{k1}^I - \zeta_{ki}^\beta T_{\mu\nu}^i \tilde{Q}_{j1}^I \tilde{Q}_{k1}^I \right] \end{aligned} \qquad [1.12]$$

However, the impact of this term on the shape of the modals is very small, but it is included within the implementation in MOLPRO by default. Self-consistent field theories relying on several Hartree products rather than a single one, for example,

vibrational multiconfiguration self-consistent field theory (VMCSCF) (Heislbetz and Rauhut 2010) or configuration-averaged vibrational self-consistent field theory (CA-VSCF) (Meisner et al. 2019), have been developed as well, but these will not be discussed in detail here.

Due to the account of anharmonicity, the modals optimized in the VSCF procedure are usually superior to simple HO functions and can be used to generate all possible Hartree products, which allow us to determine the vibrational state functions Φ_ν exactly, including vibration correlation effects, i.e.:

$$\Phi_\nu = \sum_I D_I^\nu \prod_i \varphi_i^I = \sum_I D_I^\nu \prod_i \left(\sum_\mu C_{\mu i}^I \chi_{\mu i} \right) \qquad [1.13]$$

This requires the solution of the corresponding VCI eigenvalue problem (Christoffel and Bowman 1982; Bowman et al. 1979), which apparently suffers from its huge dimension. Therefore, strategies are needed to limit the size of the correlation space (Schröder and Rauhut 2022). This can be accomplished by three criteria, that is, the maximal excitation per mode (usually values of 5 or 6 are sufficient), the maximal number of simultaneous excitations (also 5 or 6) and the maximal sum of quantum numbers for a given Hartree product (typically values of about 12 are used). This leads to tremendous reductions, but does not solve the problem. An iterative configuration selection scheme based on second-order vibrational Møller–Plesset perturbation theory (VMP2) finally limits the correlation space to those Hartree products, which are necessarily needed for a proper description of the vibrational state (Mathea et al. 2022). This approach is rooted in the same idea for electronic structure theory as originally introduced by Malrieu and co-workers (Huron et al. 1973). With the perturbation operator being given as the difference between the Watson operator and the sum of Fock-like operators, that is, $H' = H - \sum_i f_i$, the selection criterion can be written as:

$$\epsilon_{\nu I}^{(n+1)} = \frac{|\sum_{K\in\{n\}} D_K^{\nu,(n)} \langle \Psi_K | H' | \Psi_I \rangle|^2}{\epsilon_\nu^{(n)} - \epsilon_J} \qquad [1.14]$$

n denotes the iteration index and $\Phi_\nu^{(n)} = \sum_{K\in\{n\}} D_K^{\nu,(n)} |\Psi_K\rangle$ is the vibrational wavefunction of the targeted state in the nth iteration as obtained from the eigenvector of an intermediate VCI matrix in the space of the selected configurations. For the case that K runs just over one configuration (the corresponding VSCF configuration), equation [1.14] reduces to the well-known VMP2 expression. Once the energy correction of the LHS, that is, $\epsilon_{\nu I}^{(n+1)}$, is above a certain threshold, the so far unselected test configuration on the RHS of the integral, that is, Ψ_I, is added to the set of selected configurations. The iterative application of this equation arises

from the importance of indirect couplings between the configurations, which are not accounted for in standard VMP2 theory. This procedure reduces the number of configurations to be considered tremendously. An example is given in Table 1.2 for the oxirane molecule. The employed PES is that as described in Table 1.1. The experimental data were taken from the compilation of Puzzarini et al. (2014). As can be seen, the number of selected configurations scatters between 4,000 and 14,000, while the initial configuration space comprises more than 2×10^7 configurations. These were obtained from up to sextuple excitations, the sum of quantum numbers up to 15 and the maximal excitation for each mode up to the seventh root. This basis pruning led to significant CPU time savings (see Table 1.2). Note that the selection process is state specific, that is, the configuration space is tailored for an individual state of interest. As a result, for each state an individual VCI matrix needs to be set up. However, as these are independent calculations, they can be easily parallelized and in many applications the number of cores is larger than the number of states to be computed. As a result, the wall clock time for the determination of all states is often given by the most expensive calculation of an individual state. In the case of oxirane, the wall clock time for all states provided in Table 1.2 was about half an hour. The fact that only one eigenpair is needed per VCI matrix allows to employ iterative eigensolvers (Petrenko and Rauhut 2017) instead of diagonalizers, which leads to a further reduction of the CPU times (Schröder and Rauhut 2022).

Sym.	#	Exp.	VCI	Confs.	CPU (s)
A_1	ν_1	3,018.4	3,015.2	14,011	1,654
	ν_2	1,497.8	1,495.1	5,897	299
	ν_3	1,270.4	1,268.8	4,808	242
	ν_4		1,123.7	5,435	250
	ν_5	876.7	876.8	3,951	193
A_2	ν_6		3,050.9	10,419	599
	ν_7		1,155.7	4,532	178
	ν_8		1,026.3	4,853	198
B_1	ν_9	3,066.0	3,063.9	8,523	374
	ν_{10}		1,148.2	4,508	180
	ν_{11}	808.1	803.5	4,811	198
B_2	ν_{12}	3,006.5	3,003.3	10,020	622
	ν_{13}	1,471.5	1,468.0	4,469	178
	ν_{14}		1,139.2	4,893	195
	ν_{15}	822.3	822.3	4,189	166

Table 1.2. *VCI calculations for oxirane*

The iterative selection procedure and the build-up of increasingly large VCI matrices during this step require an efficient evaluation of the respective matrix elements (Mathea and Rauhut 2021; Mathea et al. 2022). The contribution of a single integral is controlled by Slater–Condon type rules, which simply requests an analysis of the quantum number vectors of the two configurations (LHS and RHS). However, the individual test for each integral is costly and the computational cost can be reduced by the introduction of configuration classes, that is, batches of configurations, which can be processed altogether.

In addition, contraction schemes can be introduced, which lead to further speed-ups. For example, the contribution of the 3D terms of the PES to an individual VCI integral can be written as:

$$H_{3D}^{IJ} = \left\langle \Psi^I | V_{3D} | \Psi^J \right\rangle \qquad [1.15]$$

$$= \sum_{i<j<k} \left(\prod_{l \neq i,j,k} \delta_{n_l^I n_l^J} \right) \sum_r \tilde{Q}_{ir}^{IJ} \sum_s \tilde{Q}_{js}^{IJ} \sum_t p_{ijk}^{(3),rst} \tilde{Q}_{kt}^{IJ} \qquad [1.16]$$

Introducing the contracted integrals:

$$X_{ijk}^{rs,IJ} = \sum_t p_{ijk}^{(3),rst} \tilde{Q}_{kt}^{IJ} \qquad [1.17]$$

which can be conveniently precomputed and stored in memory, simplifies the calculation to:

$$H_{3D}^{IJ} = \sum_{i<j<k} \left(\prod_{l \neq i,j,k} \delta_{n_l^I n_l^J} \right) \sum_r \tilde{Q}_{ir}^{IJ} \sum_s \tilde{Q}_{js}^{IJ} X_{ijk}^{rs,IJ} \qquad [1.18]$$

which clearly leads to a reduction of the operation count for each matrix element. Speed-ups between 3 and 5 were achieved by this simple trick. It is obvious that this results in larger memory demands, but these were found to be moderate and usually do not constitute a problem for customary workstations.

In summary, a bunch of techniques has been used to accelerate the calculation of vibrational wavefunctions and to represent them in a very compact form. These calculations, which provide the vibrational basis functions for the rovibrational calculations, have been fully automated and do not request any specific information from the user.

1.4. RVCI calculations

The RVCI wavefunction can be expressed in terms of products of pure vibrational and rotational basis functions, Φ_r and Φ_ν, respectively.

$$\Phi_{\text{rovib}} = \sum_{r\nu} C_{r\nu} \Phi_r \Phi_\nu \qquad [1.19]$$

VCI wavefunctions (see equation [1.13]) as obtained from a configuration-selective implementation provide a compact and optimized vibrational basis, Φ_ν, and will be used in all subsequent steps.

The rotational basis function Φ_r can be obtained from the solutions of the rigid rotor Hamiltonian. For symmetric and spherical top molecules, Φ_r is given by the symmetric top wavefunctions $|J, k, m\rangle$, which depend on the Euler angles (see Bunker and Jensen (1998)). Here, the standard notations J, k and m denote the quantum numbers associated with the angular momentum, its projection on the molecule fixed z axis and on the space fixed Z axis, respectively. For asymmetric top molecules, the rigid rotor Hamiltonian can be expressed in I^r representation as:

$$H_{\text{rot}} = \left[A - \frac{B+C}{2}\right] J_z^2 + \frac{B+C}{2}\mathbf{J}^2 + \frac{B-C}{4}\left[(J_m^+)^2 + (J_m^-)^2\right] \qquad [1.20]$$

with $J_m^\pm = J_x \pm iJ_y$ being the ladder operators. In case the last term is omitted, equation [1.20] reduces to the rotational Hamiltonian for prolate top molecules. On the other hand, if the III^r representation is considered, H_{rot} boils down to the Hamiltonian for an oblate top molecule. Asymmetric top molecules, constitute the most general case; for these linear combinations of the symmetric top functions are a suitable choice for the basis function Φ_r. A meaningful combination of rigid rotor functions supports the symmetry operations of the molecular group $\{E, R_x^\pi, R_y^\pi, R_z^\pi\}$, which is realized by Wang combinations (Wang 1929; Hills et al. 1977; Yamada 1983). Therefore, we employ Wang combinations as rotational basis functions such that (Erfort et al. 2020; Yurchenko et al. 2017):

$$|\Phi_r\rangle = \begin{cases} |J,\, 0\,, \tau = 0\rangle = |J, 0\rangle \\ |J, K, \tau = 0\rangle = \frac{1}{\sqrt{2}}(|J, K\rangle + (-1)^{J+K}|J, -K\rangle) & \text{for} \quad K \neq 0 \\ |J, K, \tau = 1\rangle = \frac{i^\sigma}{\sqrt{2}}(|J, K\rangle + (-1)^{J+K+\tau}|J, -K\rangle) & \text{for} \quad K \neq 0 \end{cases} \qquad [1.21]$$

Here, $K = |k|$ with $0 \leq K \leq J$, τ is related to the phase and $\sigma = 0$ for $\tau = 0$ and $\sigma = K \bmod 3$ for $\tau = 1$. Due to the isotropy of the space in the absence of external fields, the rotational wavefunction is independent of m. Thus, m is omitted in equation [1.21].

The rovibrational matrix becomes complex for the basis function given in equation [1.21]. However, it is possible to obtain a real rovibrational matrix for different choices of Φ_r (e.g. Špirko et al. (1985); Yurchenko et al. (2005)):

$$\begin{aligned} |J,0,\tau\rangle &= i^{\tau}|J,0\rangle \quad \text{with} \quad J+\tau = \text{even} \\ |J,K,\tau\rangle &= \frac{i^{\tau}(-1)^{\sigma}}{\sqrt{2}}(|J,K\rangle + (-1)^{J+K+\tau}|J,-K\rangle). \end{aligned} \tag{1.22}$$

Using equation [1.1], the elements of the rovibrational Hamiltonian matrix can be explicitly written as:

$$\begin{aligned} &\langle \Phi_\nu \Phi_r|(\hat{H}_{\text{rot}} + \hat{H}_{\text{cor}} + \hat{H}_{\text{vib}})|\Phi_{r'}\Phi_{\nu'}\rangle \\ &= \sum_{\alpha\beta} \frac{1}{2}\langle \Phi_\nu|\mu_{\alpha\beta}|\Phi_{\nu'}\rangle\langle \Phi_r|J_\alpha J_\beta|\Phi_{r'}\rangle \\ &- \sum_{\alpha\beta} \frac{1}{2}\langle \Phi_\nu\Phi_r|J_\alpha\mu_{\alpha\beta}\pi_\beta + \pi_\alpha\mu_{\alpha\beta}J_\beta|\Phi_{r'}\Phi_{\nu'}\rangle \\ &+ \langle \Phi_\nu|\hat{H}_{\text{vib}}|\Phi_{\nu'}\rangle\langle \Phi_r|\Phi_{r'}\rangle. \end{aligned} \tag{1.23}$$

Note that within this equation we distinguish between two different vibrational states, Φ_ν and $\Phi_{\nu'}$, which may not be confused with the configurations Ψ^I and Ψ^J as introduced in the previous chapter. Using equation [1.21], the integrals for $\hat{H}_{\text{rot}}$ over the rotational basis functions $\langle J,K,\tau|\hat{H}_{\text{rot}}|J',K',\tau'\rangle$ can be expressed in terms of the integrals $\langle J,K|\hat{H}_{\text{rot}}|J',\pm K'\rangle$. The non-vanishing integrals can only be obtained for $J = J'$. As $K = |k|$, the mathematical expression of these integrals can readily be obtained in terms of the primitive rigid rotor integrals (Papousek and Aliev 1982; Zare 1988):

$$\begin{aligned} \langle J,k|\hat{H}_{\text{rot}}|J,k\rangle =& \sum_{\alpha\beta}\frac{1}{2}\langle J,k|J_\alpha\mu_{\alpha\beta}J_\beta|J,k\rangle \\ =& \frac{1}{4}(\mu_{xx}+\mu_{yy})\{J(J+1)-k^2\} + \frac{1}{2}\mu_{zz}k^2 \end{aligned} \tag{1.24}$$

$$\langle J,k\pm 1|\hat{H}_{\text{rot}}|J,k\rangle = \frac{1}{4}[(\mu_{xz}\pm i\mu_{yz})\sqrt{J(J+1)-k(k\pm 1)}(2k\pm 1) \tag{1.25}$$

$$\begin{aligned} \langle J,k\pm 2|\hat{H}_{\text{rot}}|J,k\rangle =& \frac{1}{8}[(\mu_{xx}-\mu_{yy}\pm 2i\mu_{xy})\sqrt{J(J+1)-k(k\pm 1)} \\ &\times \sqrt{J(J+1)-(k\pm 1)(k\pm 2)}. \end{aligned} \tag{1.26}$$

Since $\mu_{\alpha\beta}$ in $\hat{H}_{\text{rot}}$ depends only on the vibrational coordinates, these terms are separated from the integrals over $|J,k\rangle$. Due to the quadratic term of J_α in $\hat{H}_{\text{rot}}$, the

integrals shown in equations [1.24]–[1.26] will be eliminated if the bra and ket vectors differ by $\Delta k > 2$. Thus, most of the integrals associated with $\hat{H}_{\text{rot}}$ are zero.

The matrix elements for the Coriolis coupling terms of the rovibrational Hamiltonian shall be considered in some more detail. Due to the symmetry of the $\boldsymbol{\mu}$-tensor and the well-known relation (Watson 1968):

$$\sum_{\alpha} \pi_{\alpha}\mu_{\alpha\beta} = \sum_{\alpha} \mu_{\alpha\beta}\pi_{\alpha} \qquad [1.27]$$

the Coriolis coupling term of the $\hat{H}_{\text{rovib}}$ can formally be rewritten to:

$$\hat{H}_{\text{cor}} = -\frac{1}{2}\sum_{\alpha\beta}[J_{\alpha}\mu_{\alpha\beta}\pi_{\beta} + \pi_{\alpha}\mu_{\alpha\beta}J_{\beta}] = -\sum_{\alpha\beta} J_{\alpha}\mu_{\alpha\beta}\pi_{\beta} \qquad [1.28]$$

However, representing the $\boldsymbol{\mu}$-tensor by a truncated n-mode expansion does not allow for the last simplification as the vibrational angular momentum operator does not commute with individual terms of the n-mode expansion. The elements of the Coriolis coupling matrix can thus be expressed as:

$$\langle \Phi_r \Phi_{\nu} | \hat{H}_{\text{cor}} | \Phi_{r'} \Phi_{\nu'} \rangle = -\frac{1}{2}\sum_{\alpha\beta} \langle \Phi_r | J_{\alpha} | \Phi_{r'} \rangle [\langle \Phi_{\nu} | \mu_{\alpha\beta}\pi_{\beta} | \Phi_{\nu'} \rangle + \langle \Phi_{\nu} | \pi_{\beta}\mu_{\alpha\beta} | \Phi_{\nu'} \rangle]. \qquad [1.29]$$

Let us consider the first integral over the vibrational wavefunctions, i.e. $\langle \Phi_{\nu} | \mu_{\alpha\beta}\pi_{\beta} | \Phi_{\nu'} \rangle$. Using equations [1.2] and [1.4] for the vibrational angular momentum operator π_{β} and an n-mode expansion of the $\boldsymbol{\mu}$-tensor fitted to polynomials, respectively, the above integral can be explicitly written as:

$$\left\langle \Phi_{\nu} \left| \left(\mu^{(0)}_{\alpha\beta} + \sum_{i,p} \mu^{(1),p}_{\alpha\beta,i} q_i^p + \sum_{i<j}\sum_{ps} \mu^{(2),ps}_{\alpha\beta,ij} q_i^p q_j^s + \cdots \right) \left(-i \sum_{kl} \zeta^{\beta}_{kl} q_k \partial_{q_l} \right) \right| \Phi_{\nu'} \right\rangle \qquad [1.30]$$

where the parameters i, j, k and l indicate vibrational modes and p and s the orders of the monomials.

For simplicity, we will also represent the n-mode expansion of the PES in terms of polynomials rather than arbitrary basis functions b_{ir} and the expression for ∂/∂_{q_j} is expressed in a simplified manner as ∂_{q_j}. The individual terms of this expression are given by:

$$\langle\Phi_\nu|\mu_{\alpha\beta}\pi_\beta|\Phi_{\nu'}\rangle_{0\mathrm{D}} = -i\sum_{kl}\zeta_{kl}^{\beta}\mu_{\alpha\beta}^{(0)}\left\langle\Phi_\nu\left|q_k\partial_{q_l}\right|\Phi_{\nu'}\right\rangle \quad [1.31]$$

$$\langle\Phi_\nu|\mu_{\alpha\beta}\pi_\beta|\Phi_{\nu'}\rangle_{1\mathrm{D}} = -i\sum_{kl}\zeta_{kl}^{\beta}\sum_{i}\sum_{p}\mu_{\alpha\beta,i}^{(1),p}\left\langle\Phi_\nu\left|q_i^p q_k\partial_{q_l}\right|\Phi_{\nu'}\right\rangle \quad [1.32]$$

$$\langle\Phi_\nu|\mu_{\alpha\beta}\pi_\beta|\Phi_{\nu'}\rangle_{2\mathrm{D}} = -i\sum_{kl}\zeta_{kl}^{\beta}\sum_{i<j}\sum_{ps}\mu_{\alpha\beta,ij}^{(2),ps}\left\langle\Phi_\nu\left|q_i^p q_j^s q_k\partial_{q_l}\right|\Phi_{\nu'}\right\rangle \quad [1.33]$$

$$\langle\Phi_\nu|\mu_{\alpha\beta}\pi_\beta|\Phi_{\nu'}\rangle_{3\mathrm{D}} = \ldots \quad [1.34]$$

Expressing Φ_ν as a linear combination of VSCF configurations (see equation [1.13]) and defining the integrals $\tilde{Q}_{ip}^{IJ}$ by rewriting equation [1.7] for different VCI configurations:

$$\tilde{Q}_{ip}^{IJ} = \langle\varphi_i^I|q_i^p|\varphi_i^J\rangle = \sum_{\mu\nu}C_{\mu i}^I C_{\nu i}^J Q_{\mu\nu}^{ip} \quad [1.35]$$

as well as

$$\Delta_{ip}^{IJ} = \langle\varphi_i^I|q_i^p\partial_{q_i}|\varphi_i^J\rangle, \quad [1.36]$$

leads to the working equation for the $\langle\Phi_\nu|\mu_{\alpha\beta}\pi_\beta|\Phi_{\nu'}\rangle_{0D}$ term:

$$\langle\Phi_\nu|\mu_{\alpha\beta}\pi_\beta|\Phi_{\nu'}\rangle_{0\mathrm{D}} = -i\sum_{kl}\zeta_{kl}^{\beta}\mu_{\alpha\beta}^{(0)}\sum_{IJ}D_I^\nu D_J^{\nu'}\tilde{Q}_{k1}^{IJ}\Delta_{l0}^{IJ}\delta_{kl}^{IJ} \quad [1.37]$$

with

$$\delta_{kl}^{IJ} = \prod_{i\neq k,l}\langle\varphi_i^I|\varphi_i^J\rangle. \quad [1.38]$$

Note that $\zeta_{kl}^{\beta} = 0$ for $k = l$. Despite the dependence on I and J, the integrals $\tilde{Q}_{ip}^{IJ}$ can be easily stored in memory as they depend on just one coordinate i.

Likewise, the integrals $\langle\Phi_\nu|\mu_{\alpha\beta}\pi_\beta|\Phi_{\nu'}\rangle_{1D}$ can be expressed in a similar manner, but different cases with respect to the normal modes need to be distinguished:

1) $i = k \neq l$:

$$\langle\Phi_\nu|\mu_{\alpha\beta}\pi_\beta|\Phi_{\nu'}\rangle_{1\mathrm{D}} = -i\sum_{il}\sum_{p}\mu_{\alpha\beta,i}^{(1),p}\zeta_{il}^{\beta}\sum_{IJ}D_I^\nu D_J^{\nu'}\tilde{Q}_{i(p+1)}^{IJ}\Delta_{l0}^{IJ}\delta_{il}^{IJ} \quad [1.39]$$

2) $k \neq l = i$:

$$\langle\Phi_\nu|\mu_{\alpha\beta}\pi_\beta|\Phi_{\nu'}\rangle_{1\mathrm{D}} = -i\sum_{ik}\sum_{p}\mu_{\alpha\beta,i}^{(1),p}\zeta_{ki}^{\beta}\sum_{IJ}D_I^\nu D_{I'}^{\nu'}\tilde{Q}_{k1}^{IJ}\Delta_{ip}^{IJ}\delta_{ik}^{IJ} \quad [1.40]$$

3) $i \neq k \neq l$:

$$\langle \Phi_\nu | \mu_{\alpha\beta} \pi_\beta | \Phi_{\nu'} \rangle_{1D} = -i \sum_{ikl} \sum_p \mu^{(1),p}_{\alpha\beta,i} \zeta^\beta_{kl} \sum_{IJ} D^\nu_I D^{\nu'}_J \tilde{Q}^{IJ}_{ip} \tilde{Q}^{IJ}_{k1} \Delta^{IJ}_{l0} \delta^{IJ}_{ikl}. \quad [1.41]$$

δ^{IJ}_{ikl} is defined similar to equation [1.38]:

$$\delta^{IJ}_{ikl} = \prod_{j \neq i,k,l} \langle \varphi^I_j | \varphi^J_j \rangle. \quad [1.42]$$

The second term in equation [1.29], i.e. the integral $\langle \Phi_\nu | \pi_\beta \mu_{\alpha\beta} | \Phi_{\nu'} \rangle$, leads again to the same integrals for the zeroth and first-order terms of the $\boldsymbol{\mu}$-tensor except for the case $k \neq l = i$, i.e.:

$$k \neq l = i :$$

$$\langle \Phi_\nu | \pi_\beta \mu_{\alpha\beta} | \Phi_{\nu'} \rangle_{1D} = -i \sum_{ik} \sum_p \zeta^\beta_{ki} \mu^{(1),p}_{\alpha\beta,i} \sum_{IJ} D^\nu_I D^{\nu'}_J \tilde{Q}^{II'}_{k1} (p \tilde{Q}^{IJ}_{i(p-1)} + \Delta^{IJ}_{ip}) \delta^{IJ}_{ik}. \quad [1.43]$$

The additional contribution of $p\tilde{Q}^{IJ}_{i(p-1)}$ due to the product rule (see equation [1.43]), in comparison to equation [1.40] readily explains why equation [1.28] cannot be applied once a truncated $\boldsymbol{\mu}$-tensor expansion has been used. For the terms of higher order, that is, 2D, the integrals can be evaluated accordingly and in principle even more cases have to be considered. However, it can be shown that in all arising cases for the high-order terms only four different integrals need to be considered, which renders the implementation quite easy.

The rotational integral arising from $\hat{H}_{cor}$ is fairly simple. It is zero if the k-quantum numbers in the bra and ket wavefunctions differ by $\Delta k > 1$. Therefore, only three cases need to be considered:

$$\langle J, k | J_z | J, k \rangle = k \quad [1.44]$$

$$\langle J, k \pm 1 | J_x | J, k \rangle = \pm i \langle J, k \pm 1 | J_y | J, k \rangle \quad [1.45]$$

$$= \frac{1}{2} \sqrt{J(J+1) - k(k \pm 1)}. \quad [1.46]$$

With that, the Coriolis terms can be computed straightforwardly. A detailed schematic description of the vibrational, rotational and Coriolis terms in a rovibrational matrix is given below. The indices of the superscript of H_{vib} indicate the vibrational quantum numbers, that is, $H^{\nu_i \nu_j}_{vib}$. For H_{rot} and H_{cor}, the first and second pair of indices, separated by a comma, indicate the vibrational and rotational quantum numbers, that is, $H^{\nu_i \nu_j, r_i r_j}_{rot}$ and $H^{\nu_i \nu_j, r_i r_j}_{cor}$, respectively.

$$
\begin{pmatrix}
\begin{pmatrix} H_{\text{vib}}^{00} + H_{\text{rot}}^{00,00} & H_{\text{rot}}^{00,01} & \cdots \\ H_{\text{rot}}^{00,10} & H_{\text{vib}}^{00} + H_{\text{rot}}^{00,11} & \cdots \\ \vdots & \vdots & \ddots \end{pmatrix} &
\begin{pmatrix} H_{\text{cor}}^{01,00} + H_{\text{rot}}^{01,00} & H_{\text{cor}}^{01,01} + H_{\text{rot}}^{01,01} & \cdots \\ H_{\text{cor}}^{01,10} + H_{\text{rot}}^{01,10} & H_{\text{cor}}^{01,11} + H_{\text{rot}}^{01,11} & \cdots \\ \vdots & \vdots & \ddots \end{pmatrix} & \cdots \\
\begin{pmatrix} H_{\text{cor}}^{10,00} + H_{\text{rot}}^{10,00} & H_{\text{cor}}^{10,01} + H_{\text{rot}}^{10,01} & \cdots \\ H_{\text{cor}}^{10,10} + H_{\text{rot}}^{10,10} & H_{\text{cor}}^{10,11} + H_{\text{rot}}^{10,11} & \cdots \\ \vdots & \vdots & \ddots \end{pmatrix} &
\begin{pmatrix} H_{\text{vib}}^{11} + H_{\text{rot}}^{11,00} & H_{\text{rot}}^{11,01} & \cdots \\ H_{\text{rot}}^{11,10} & H_{\text{vib}}^{11} + H_{\text{rot}}^{11,11} & \cdots \\ \vdots & \vdots & \ddots \end{pmatrix} & \cdots \\
\vdots & \vdots & \ddots
\end{pmatrix}
$$

Rovibrational wavefunctions Φ_{rovib} with different J-quantum numbers or belonging to different irreducible representations (irreps) do not interact with each other through H_{rovib}. Consequently, it is possible to construct an RVCI matrix, which is block diagonal with respect to the J-quantum number and the irreps of the molecule. A schematic of the block structured rovibrational matrix (for the C_{2v} point group) is shown in Figure 1.1. The block structure reduces the computational effort considerably by avoiding the construction of a higher dimensional matrix, which needs to be diagonalized. Besides this, it allows for a very efficient parallelization of the code.

The dimension of the rovibrational basis, which is given by $(2J+1)N_{\text{vib}}$, grows rapidly depending on the number of vibrational basis functions and the angular momentum quantum number. Therefore, both values must be kept as small as possible without losing any accuracy. Polyadic schemes have been used to limit the vibrational basis, but for asymmetric top molecules or larger molecules, these were found to be unreliable (Aliev and Watson 1985; Herman and Perry 2013; Rey 2022). Alternatively, one may limit the number of vibrational states to be included by the sum of the quantum numbers and lower/upper bounds with respect to the transition energy. For many applications, it was found to be sufficient to limit the sum of quantum numbers of the states to be included to three and to limit the energetical range of these states to the spectral range ± 500 cm^{-1}. More advanced basis pruning concepts are subject of current research. For a given temperature, the maximal value for J, that is, J_{max}, can conveniently be determined from the convergence of the rotational partition function and thus it just depends on a simple threshold.

In order to identify the energy levels and transitions, it is necessary to assign the quantum numbers of the eigenstates of the rovibrational matrix. Due to the block diagonal structure of H_{rovib}, there is no mixing of the J-quantum numbers and the irreducible representations as a result of the diagonalization. Consequently, these quantities are *good* quantum numbers and all states can be correctly labeled with

respect to them. For prolate and oblate symmetric top molecules, K_a or K_c, respectively, are also good quantum numbers. K_a and K_c are defined by the z-component of the angular momentum operator (J_z) as follows: for a prolate molecule, $J_z |\Phi_r\rangle = K_a |\Phi_r\rangle$; for an oblate molecule, $J_z |\Phi_r\rangle = K_c |\Phi_r\rangle$. However, due to the anharmonicity of the PESs, centrifugal distortion and Coriolis coupling effects, ν and K are not good quantum numbers for asymmetric top molecules. Consequently, it is not trivial to identify the K and ν quantum numbers for a given state and even the assignment is a questionable task (Mathea and Rauhut 2020), that is, what is the meaning of assigning an integer quantum number, if its real percentage is very low? In that case, the state identity cannot be expressed in terms of simple quantum numbers. The K-quantum number can be assigned by summing up the squares of the absolute values of the coefficients for which ν is largest. Likewise, ν can be determined. However, it is rather obvious that for strongly coupled states, this procedure may be troublesome.

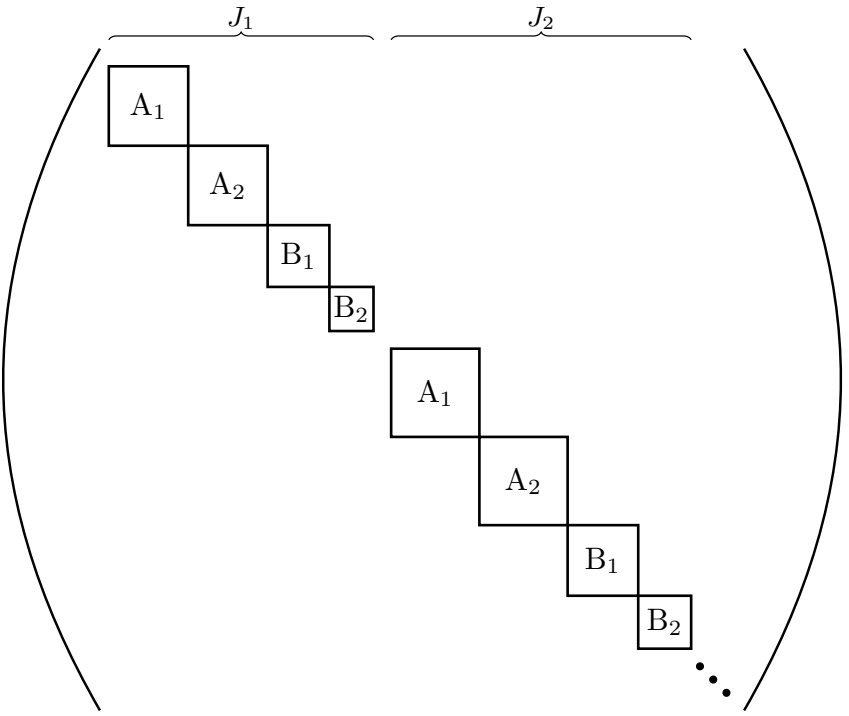

Figure 1.1. *Schematic of a block structured rovibrational matrix due to point group symmetry. Symmetry blocks for arbitrary angular momenta with $J_1 < J_2$ are considered*

Depending on the molecular systems, it is frequently observed that the eigenvectors of the rovibrational matrix are extremely sparse, particularly for larger values of the J-quantum number. The storage of this sparse rovibrational eigenvector matrix in a two-dimensional array has a significant negative impact on the computational efficiency for further calculations. Besides this, by exploiting sparsity many more vectors belonging to different values of J can be kept in memory at the same time, which may avoid their storage on disk. It is therefore meaningful to store only important elements of the eigenvectors. Several approaches are available to achieve this, including the use of a coordinate storage format, a compressed sparse row (CSR) format or a compressed sparse column (CSC) format (Duff et al. 1989; Langr and Tvrdík 2016). In this work, a CSC format was used to store the rovibrational eigenvectors. The sparsity factor or simply sparsity of a matrix of the rovibrational eigenfunctions can be defined as:

$$\text{sparsity} = 1 - \frac{\text{total non-negligible elements}}{\text{total number of elements}}. \quad [1.47]$$

Figure 1.2 shows that the sparsity factor is almost negligible for small values of the angular momentum quantum number J. After a certain value or cut-off, the sparsity increases with J. For very large values of J, the curves asymptotically approach a certain limit. Note that for $J = 0$, the rovibrational eigenfunctions show only contributions from the vibrational wavefunctions, which causes most of the elements in the matrix to vanish. The dependence of the sparsity on the corresponding thresholds is also shown in Figure 1.2 for values ranging from $10^{-4}/(J + 1)$ to $10^{-10}/(J + 1)$. As the eigenfunctions are normalized, the coefficients may be distributed over very many elements for larger values of the J-quantum number, which can lead to smaller coefficients in general. To account for this effect, the division by J is introduced.

The computational benefits due to the consideration of the block diagonal structure of the rovibrational matrices and the exploitation of sparsity are shown in Table 1.3 for two molecules (Das and Rauhut 2024). The chosen program parameters for H_2CCS (C_{2v}) are: $N_{\text{vib}} = 43$, $J_{\text{max}} = 100$, $N_{\text{Cores}} = 15$, and for HCSCN (C_s): $N_{\text{vib}} = 14$, $J_{\text{max}} = 100$, $N_{\text{Cores}} = 24$. For both molecules, the μ-tensor has been expanded up to the 2D and 1D terms for the rotational and Coriolis contributions of the Hamiltonian, respectively. The threshold for the sparsity was chosen to be $10^{-6}/(J + 1)$ for both molecules. Due to symmetry blocking, the CPU time is reduced by factors of almost 4.8 and 2.1 for H_2CCS and HCSCN, respectively. As the order of the point group of H_2CCS is 4, while it is 2 for HCSCN, the symmetry blocking reduces the CPU time for the former molecule much more than for HCSCN. Taking into account sparsity, the CPU time is further reduced by a factor of about 1.5 and 2.9 for H_2CCS and HCSCN, respectively, and thus an overall acceleration by almost an order of magnitude can be achieved. The latter reduction arises exclusively

from the calculation of the rovibrational intensities as the sparsity techniques are applied after the diagonalization of the RVCI matrices. As both, the symmetry blocking and the sparsity techniques, reduce also the memory requests of the corresponding calculations, the number of cores being used can be increased, which has not been shown in Table 1.3 to avoid overlaying two effects.

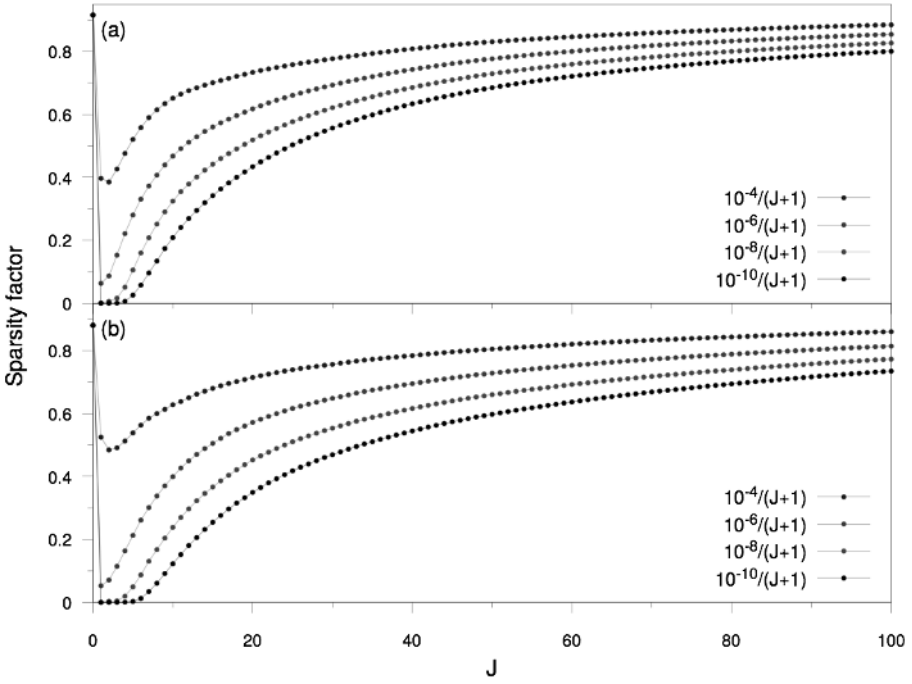

Figure 1.2. *Variation of the sparsity in the eigenfunctions of rovibrational matrices with respect to the total angular momentum quantum number (J) for (a) thioketene (H_2CCS) and (b) thioformyl cyanide (HCSCN). Curves for different choices of the sparsity threshold are shown in different colors. For a color version of this figure, see www.iste.co.uk/rey/molecularspectroscopy1B.zip*

Molecule	Symmetry	Sparsity factor	Computational time (min)		
			No sym. block	Sym. block	Sparsity
H_2CCS	C_{2v}	0.85	190	40	26
HCSCN	C_s	0.81	131	61	21

Table 1.3. *The impact of symmetry and sparsity on the CPU times for H_2CCS and HCSCN. Computational details are provided in the text body*

As the rovibrational states energies depend on the order of the n-mode expansion of the $\boldsymbol{\mu}$-tensor (see equation [1.4]) occurring in the H_{rot} and H_{cor} terms, an analysis of the expansions of the $\boldsymbol{\mu}$-tensor is mandatory. For simplicity, let us denote the truncation orders of the $\boldsymbol{\mu}$-tensor within H_{rot} and H_{cor} as $\mathcal{O}(\mu_{\text{rot}})$ and $\mathcal{O}(\mu_{\text{cor}})$, respectively. Table 1.4 displays the CPU times and root mean square deviations (RMSD) of a set of about 1.5×10^5 eigenvalues for different values of $\mathcal{O}(\mu_{\text{rot}})$ and $\mathcal{O}(\mu_{\text{cor}})$. All data refer to the HCSCN molecule (C_s) with $N_{\text{vib}} = 14$, $J_{\text{max}} = 100$ and $N_{\text{Cores}} = 24$. The reference calculation was chosen to employ $\mathcal{O}(\mu_{\text{rot}}) = 3$ and $\mathcal{O}(\mu_{\text{cor}}) = 2$. It is easy to see that the inclusion of the 2D terms of the $\boldsymbol{\mu}$-tensor for the Coriolis contributions increases the CPU time tremendously. However, this arises mainly from the fact, that the algorithm for these terms has not yet been optimized. Contrarily, if Coriolis coupling is neglected completely, i.e. $H_{\text{cor}} = 0$, the RMSD grows relatively large. This indicates that the Coriolis coupling between the rovibrational states is quite strong. In general and as observed in studies for different molecules (Tschöpe and Rauhut 2022), for certain applications the Coriolis contributions appear to be sufficiently converged for $\mathcal{O}(\mu_{\text{cor}}) = 1$, while an additional order, that is, $\mathcal{O}(\mu_{\text{rot}}) = 2$, appears to be necessary for the rotational terms (see, for example, Dinu et al. (2022)). Of course, these parameters will vary for troublesome molecules, but may serve as an initial guess for many applications.

$\mathcal{O}(\mu_{\text{rot}})$ \ $\mathcal{O}(\mu_{\text{cor}})$	None		0D		1D		2D	
0D	239.389	(4)	233.730	(16)	233.059	(18)	233.027	(63)
1D	15.869	(8)	10.090	(20)	8.364	(22)	8.359	(71)
2D	13.398	(8)	6.168	(20)	0.387	(21)	0.096	(72)
3D	13.393	(8)	6.163	(24)	0.377	(22)	Ref.	(69)

Table 1.4. *Root mean square deviations (RMSD) of RVCI eigenvalues with respect to a reference calculation for different orders of the n-mode expansions of the $\boldsymbol{\mu}$-tensor within H_{rot} and H_{cor} terms, that is, $\mathcal{O}(\mu_{rot})$ and $\mathcal{O}(\mu_{cor})$, respectively, for HCSCN. Numbers in parentheses refer to CPU times in minutes for the corresponding calculations*

1.5. Infrared intensities

As the calculation of rovibrational state energies provides just one half of the information being needed for the simulation of a spectrum the calculation of intensities is mandatory. Within MOLPRO, both infrared and Raman intensities have been implemented, but in the following we will exclusively focus on the former. The absorption intensity of a rovibrational transition from an initial state ($''$) to a final state ($'$) can be expressed as:

$$I = C\, e^{-E''/k_B T}\, \frac{1 - e^{-(E'-E'')/k_B T}}{Q(T)} (E' - E'') S(\mu) \qquad [1.48]$$

with $S(\mu)$ being the line strength due to a transition from the initial to the final state. While C summarizes some natural constants and factors, T and k_B are the temperature and the Boltzmann constant, respectively. The partition function $Q(T)$ associated with the rovibrational states can be expressed as:

$$Q(T) = \sum_j g_j e^{-E_j/k_B T} \qquad [1.49]$$

where E_j denotes the rovibrational energy of the jth state and g_j is its corresponding degeneracy. In principle, $Q(T)$ can be computed from the eigenstates of an RVCI calculation as described above. However, the RVCI calculation for high-lying rovibrational states is a computationally demanding task and may not be needed for many applications. As a result, the sum over states remains incomplete and the partition function inaccurate. We employ a separability approximation within calculations without any external fields and thus a simple product form is used in our implementation (Chakraborty et al. 2004; Owens et al. 2017; Yurchenko et al. 2018):

$$Q(T) = \underbrace{\left(\sum_\nu g_\nu e^{-E_\nu/k_B T}\right)}_{Q_v} \underbrace{\sum_r g_{ns}^r (2J_r + 1) e^{-E_r/k_B T}}_{Q_r} \qquad [1.50]$$

g_{ns}^r denotes degeneracies related to the nuclear spin, which can conveniently be computed from the Landau–Lifshitz formula (Landau and Lifshitz 1977) for each irrep. Note that the second term of this product is not the bare rotational partition function as it includes the weighting by g_{ns}^r. Q_v is the vibrational partition function.

Q_r can approximately be obtained from an RVCI calculation solely including the vibrational ground state. Moreover, Coriolis terms are neglected and the n-mode expansion of the $\boldsymbol{\mu}$-tensor for H_{rot} is truncated after the zeroth-order term. These very fast RVCI calculations with increasing values for J lead to a curve for Q_r, which asymptotically approaches a limit. Once the changes arising from increasing values for J were found to be below a certain threshold, the determination of Q_r stops. As outlined above, this procedure can be used to determine J_{max} for a given temperature.

On the other hand, the number of vibrational states increases rapidly with the number of mode-specific basis functions, $\chi_{\mu i}$, and the number of vibrational modes. Inclusion of all states, which can be generated from these, is not only a very demanding task, but also irrelevant for rovibrational calculations. However, the energy of excited states, which are not exclusively considered in the preceding VCI calculations, can be adequately approximated by the VSCF modal energies, that is:

$$E_\nu \approx \sum_i \varepsilon_i^\nu \qquad [1.51]$$

where ε_i^ν is the modal energy of the ith mode for the vibrational state ν. However, even the account of all states by this simple formula would be demanding and thus the

summation is restricted arising from energy bounds and upper limits for the vibrational quantum numbers. Deviations with respect to accurately computed partition functions were found to be very low.

In a very general manner, the line strength can be expressed as:

$$S(\mu) = \sum_{\Phi',\Phi''} \sum_{\alpha\in X,Y,Z} |\langle\Phi'|\mu_\alpha|\Phi''\rangle|^2 \qquad [1.52]$$

and within a separability approximation for the electronic and nuclear spin functions, the former being based on the Born–Oppenheimer approximation, the wavefunctions Φ' and Φ'' are simply products of the nuclear spin, electronic and rovibrational functions.

However, for rovibrational transitions within a single electronic state the initial and final electronic and nuclear spin wavefunctions are identical. The first summation in equation [1.52] accounts for the degeneracies of the initial and final states and the Cartesian components, μ_α, of the dipole moment refer to the space fixed coordinate system. Integrals of dipole moments in the basis of rovibrational functions can be conveniently obtained in terms of their irreducible spherical tensor components instead of their Cartesian components and thus they need to be transformed accordingly (Papousek and Aliev 1982; Yurchenko 2023):

$$\tilde{\mu}_s^{(1,\sigma)} = \sum_{\sigma'=-1}^{1} [D^{(1)}_{\sigma,\sigma'}]^* \underbrace{\sum_{\alpha\in x,y,z} U_{\sigma',\alpha}\langle\Phi_{\text{elec}'}|\mu_\alpha|\Phi_{\text{elec}'}\rangle}_{\tilde{\mu}_m^{(1,\sigma')}} \qquad [1.53]$$

with $\tilde{\mu}_m^{(1,\sigma')}$ denoting the molecule fixed rank 1 spherical tensor of the dipole moments and **U** being a unitary matrix:

$$U_{\sigma',\alpha} = \frac{1}{\sqrt{2}} \begin{pmatrix} 1 & -i & 0 \\ 0 & 0 & \sqrt{2} \\ -1 & -i & 0 \end{pmatrix}, \qquad [1.54]$$

which transforms the Cartesian components into the spherical ones (-1,0,1). The Wigner rotation matrix elements $D^{(1)}_{\sigma\sigma'}$ are functions of the Euler angles (Zare 1988). Clearly, the occurrence of the electronic dipole integrals in the electronic basis requires the availability of DMSs as can be obtained from electronic structure calculations. These are constructed the same way as the PES and are expressed in terms of an n-mode expansion. Once high accuracy is requested, the analytical calculation of the DMS can be very demanding. For example, the solution of the coupled-perturbed coupled-cluster equations is roughly as expensive as the determination of the corresponding energy. With that the determination of a DMS at

the correlated level is a demanding task, while their calculation at the Hartree–Fock level is a by-product of the PES generation. However, as explained above for PESs, efficient multi-level schemes can be used to limit the computational effort.

Consequently, the line strength can be expressed in terms of the spherical tensor components of the dipole moment expectation values as:

$$S(\mu) = g_{ns} \sum_{\Phi'_{\text{rovib}} \Phi''_{\text{rovib}}} \sum_{\sigma=-1}^{1} \left| \sum_{\sigma'=-1}^{1} \langle \Phi'_{\text{rovib}} | [D^{(1)}_{\sigma\sigma'}]^* \tilde{\mu}^{(1,\sigma')}_m | \Phi''_{\text{rovib}} \rangle \right|^2 \quad [1.55]$$

with g_{ns} accounting for the nuclear spin degeneracy. Substituting equation [1.19] using arbitrary rotational basis functions and lifting any vibrational degeneracies yields:

$$S(\mu) = g_{ns} \sum_{\Phi_{r'} \Phi_{r''}} \sum_{\sigma=-1}^{1} \left| \sum_{\sigma'=-1}^{1} \sum_{r',r''} \sum_{\nu',\nu''} (C'_{r\nu})^* C''_{r\nu} \right.$$
$$\left. \times \langle \Phi_{r'} \Phi_{\nu'} | [D^{(1)}_{\sigma\sigma'}]^* \tilde{\mu}^{(1,\sigma')}_m | \Phi_{r''} \Phi_{\nu''} \rangle \right|^2. \quad [1.56]$$

Introducing simple rigid rotor basis functions and considering a transition between rovibrational states being characterized by J' and J'' leads to:

$$S(\mu) = g_{ns} \sum_{m',m''} \sum_{\sigma=-1}^{1} \left| \sum_{\sigma'=-1}^{1} \sum_{k',k''} \sum_{\nu',\nu''} (C'_{Jk\nu})^* C''_{Jk\nu} \right.$$
$$\left. \times \langle J'k'm' | [D^{(1)}_{\sigma\sigma'}]^* | J''k''m'' \rangle \langle \Phi_{\nu'} | \tilde{\mu}^{(1,\sigma')}_m | \Phi_{\nu''} \rangle \right|^2 \quad [1.57]$$

where the coefficients $(C'_{Jk\nu})^*$ and $C''_{Jk\nu}$ denote the elements of the corresponding RVCI eigenvectors of the matrix blocks belonging to J' and J'' and $\langle \Phi_{\nu'} | \tilde{\mu}^{(1,\sigma')}_m | \Phi_{\nu''} \rangle$ are the dipole integrals in the basis of the VCI states. With:

$$|Jkm\rangle = \sqrt{\frac{2J+1}{8\pi^2}} [D^J_{mk}]^* \quad [1.58]$$

and according to Zare (1988), the integrals over the rotation matrix element $[D^{(1)}_{\sigma\sigma'}]^*$ can be expressed by Wigner 3-j symbols as both quantities are related to the Clebsch–Gordan coefficients. Straightforward exploitation of the properties of the 3-j symbols finally yields:

$$S(\mu) = g_{ns}(2J''+1)(2J'+1) \left| \sum_{\sigma'=-1}^{1} (-1)^{\sigma'} \sum_{\nu',\nu''} \langle \Phi_{\nu'} | \tilde{\mu}^{(1,\sigma')}_m | \Phi_{\nu''} \rangle \right.$$
$$\left. \times \sum_{k',k''} (-1)^{k''} (C'_{\nu Jk})^* C''_{\nu Jk} \begin{pmatrix} J'' & 1 & J' \\ k'' & \sigma' & -k' \end{pmatrix} \right|^2. \quad [1.59]$$

The prefactors $(2J+1)$ simply arise from the absence of any external fields. This equation essentially is the working equation for rigid rotor functions. In the case of infrared intensities, the Wigner 3-j symbols $\begin{pmatrix} J_1 & J_2 & J_3 \\ M_1 & M_2 & -M_3 \end{pmatrix}$ do not vanish once the following conditions (Messiah 1962; Shore and Menzel 1968; Lai 1994):

1) $-|J_i| \leq M_i \leq |J_i| \quad \text{for} \quad i \in \{1,2,3\} \quad \text{and} \quad J_2 = 1$

2) $M_1 + M_2 = M_3$

3) $|J_1 - 1| \leq J_3 \leq J_1 + 1$

are fulfilled. These conditions lead to the selection rules for J and k. Besides directly providing the relation between J and k-quantum numbers, the first condition also implies that the range of σ' is from -1 to +1. The second condition indicates that a transition is feasible for $\sigma' = k' - k''$, which can be expressed as the selection rule $|k' - k''| \leq 1$. Moreover, the third condition leads to the selection rule for a transition that $\Delta J = 0, \pm 1$.

However, as outlined above, rigid rotor functions are not the best choice within RVCI calculations and usually Wang combinations are employed. In that case, the expression for the line strength becomes slightly more complicated, i.e.:

$$S(\mu) = g_{ns}(2J''+1)(2J'+1)\Big| \sum_{\sigma'=-1}^{1} (-1)^{\sigma'} \sum_{\nu',\nu''} \langle \Phi_{\nu'} | \tilde{\mu}_m^{(1,\sigma')} | \Phi_{\nu''} \rangle \sum_{(K\tau)',(K\tau)''} (-1)^{K''}$$
$$\times (C'_{\nu JK\tau})^* C''_{\nu JK\tau} \sum_{\tilde{\tau}',\tilde{\tau}''} (t'_{\tilde{\tau},JK\tau})^* t''_{\tilde{\tau},JK\tau} \begin{pmatrix} J'' & 1 & J' \\ (-1)^{\tilde{\tau}''} K'' & \sigma' & (-1)^{\tilde{\tau}'+1} K' \end{pmatrix} \Big|^2 \qquad [1.60]$$

with $t'_{\tilde{\tau},JK\tau}$ and $t''_{\tilde{\tau},JK\tau}$ denoting the Wang coefficients. The probability of a transition depends on the population of the initial state that follows the Maxwell–Boltzmann distribution. A feasible hot band transition may be considered once the initial vibrational state shows a population larger than 5% of the maximally populated vibrational state. This value was found to be low enough to limit the significantly increasing computational effort arising from the inclusion of hot bands, while capturing the most important contributions to the spectrum.

This is the basic theory being implemented in the MOLPRO package for calculating rovibrational state energies and infrared intensities. The calculation of the latter can be quite demanding, but profits considerably from the sparsity concepts discussed above, which leads to a substantial reduction of the loop lengths. As an example of such a calculation, the rovibrational infrared spectra of HCSCN corresponding to the fundamental band ν_5 are shown in Figure 1.3. These are obtained for different choices of the truncation order of the $\boldsymbol{\mu}$-tensor within the Coriolis terms, while the expansion

of the $\boldsymbol{\mu}$-tensor for the rotational terms is always truncated after 2D. The lower two spectra look very similar, whereas the upper two show distinct differences and must thus be considered not converged with respect to H_{cor}.

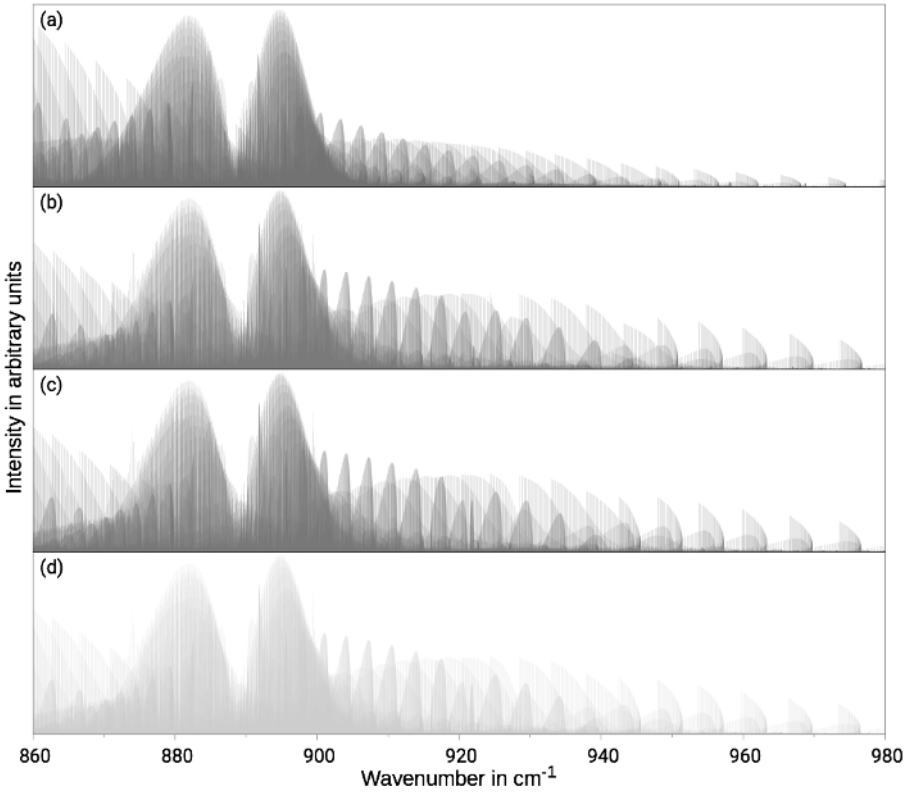

Figure 1.3. *The rovibrational spectra of HCSCN for (a) $\mathcal{O}(\mu_{cor}) =$ None and different orders of the n-mode expansion of the $\boldsymbol{\mu}$-tensor for the Coriolis coupling terms, that is, (b) 0D, (c) 1D and (d) 2D. The expansion of the $\boldsymbol{\mu}$-tensor in the H_{rot} term is fixed to 2D. The rovibrational spectra correspond to the region around the fundamental band ν_5. For a color version of this figure, see www.iste.co.uk/rey/molecularspectroscopy1B.zip*

1.6. Conclusion and outlook

The calculation of rovibrational spectra requires the control of many aspects and relies on a balanced description of several intermediate quantities. The most impactful component entering these calculations is the PES, and high-level electronic structure calculations are mandatory to obtain qualitatively correct results. However, recent progress in the construction of multidimensional PESs allows, nowadays, the

calculation of molecules with perhaps up to 12 atoms in routine applications, but for systems with more than six atoms the multi-level approximations appear to be mandatory (Schröder and Rauhut 2024). These calculations profit considerably from modern multi-core architectures, and if progress in that direction continues, even larger molecules appear to be in range.

```
basis=vqz                          Basis set for electronic structure
                                     calculation

rhf                                Hartree-Fock calculation
ccsd(t)                            Coupled-cluster calculation
optg                               Geometry optimization for determining
                                     the equilibrium structure
freq                               Harmonic frequency calculation

label1                             Definition of electronic structure level
rhf                                  for the PES
{ccsd(t)
 cphf,1}                           Calculation of analytical dipole moments

{xsurf,start1D=label1              PES calculation starting at label1
 intensity,dipole=2                Dipole moment surface calculation
 disk,dump='PES.pot'}              Dump PES on disk

vibstate,combi=3,ubound=1200       Vibrational states to be included
poly                               Transform PES to polynomials
vscf,pot=poly                      Perform VSCF calculation
{vci,pot=poly                      Perform VCI calculation
 rovib,dump_IR='line_list.dat'}    Perform RVCI calculation and store
                                     line list on disk
```

Figure 1.4. MOLPRO *input for the calculation of a PES represented by polynomials, a vibrational spectrum at the VCI level and a subsequent RVCI calculation, which dumps the line list to disk*

Concerning the vibrational structure calculations, a bottleneck is given by the calculation of strongly coupled and high-lying vibrational states as the configuration selection techniques are less efficient in these cases. However, for rovibrational calculations in the field of astrochemistry, which often deals with very low temperatures, for example, as prevalent in the interstellar medium, mainly low-lying vibrational states need to be considered, which can almost exclusively be computed in all cases. These VCI calculations have been automated to large extent and little expert knowledge is needed nowadays to yield reliable results. The same holds true for the rovibrational RVCI calculations, which appear to be less mature than the underlying VCI calculations and thus recent research activities focus on improvements regarding this part. Figure 1.4 shows a simple example of a rovibrational calculation using MOLPRO, which just requests an approximate input geometry for the molecule of interest and a bunch of keywords. This calculation,

which includes a complete determination of the PES and DMS using a single electronic structure level, and which relies very much on default parameters, clearly can also be handled by non-experts, but of course all parts need to be controlled whether the results are properly converged or not. Many techniques have been implemented in such a way that the program controls itself and very many parameters, for example, the maximal order for the polynomial basis or the size of the correlation space, are determined in an automated manner, but of course can be overwritten by a user-defined input. Nevertheless, further developments concerning the reduction of the computational demands, the handling of floppy molecules or molecular cluster, the calculation of spectra for high temperatures, and so on are the subject of current research and will accompany us within the next decade.

1.7. Acknowledgments

The authors thank the Deutsche Forschungsgemeinschaft for continuous support and, in particular, for the research project Ra 656/32-1. Moreover, G.R. thanks his former PhD students Sebastian Erfort and Martin Tschöpe for the effort they put into the development of the first versions of this program, and Benjamin Schröder for critically reading the initial draft of this contribution.

1.8. References

Aliev, M.R. and Watson, J.K.G. (1985). Higher-order effects in the vibration-rotation spectra of semirigid molecules. In *Molecular Spectroscopy: Modern Research*, volume 3, Rao, K.N. (ed.). Academic Press, London.

Bowman, J.M. (1978). Self-consistent field energies and wavefunctions for coupled oscillators. *J. Chem. Phys.*, 68, 608–610.

Bowman, J.M., Christoffel, K., Tobin, F. (1979). Application of SCF-CI theory to vibrational motion in polyatomic molecules. *J. Phys. Chem.*, 83, 905–912.

Bowman, J.M., Carrington, T., Meyer, H.-D. (2008). Variational quantum approaches for computing vibrational energies of polyatomic molecules. *Mol. Phys.*, 106(16–18), 2145–2182.

Bunker, P.R. and Jensen, P. (1998). *Molecular Symmetry and Spectroscopy*. NRC Research Press, Ottawa.

Carney, G.D., Sprandel, L.L., Kern, C.W. (1978). Variational approaches to vibration-rotation spectroscopy for polyatomic molecules. In *Advances in Chemical Physics*, volume 37, Prigogine, I. and Rice, S.A. (eds). John Wiley & Sons, Inc., New York.

Chakraborty, A., Truhlar, D.G., Bowman, J.M., Carter, S. (2004). Calculation of converged rovibrational energies and partition function for methane using vibrational-rotational configuration interaction. *J. Chem. Phys.*, 121, 2071–2084.

Christoffel, K.M. and Bowman, J.M. (1982). Investigations of self-consistent field, SCF CI and virtual state configuration-interaction vibrational energies for a model 3-mode system. *Chem. Phys. Lett.*, 85, 220–224.

Das, S. and Rauhut, G. (2024). Acceleration of rovibrational spectrum calculations through sparsity techniques. *J. Chem. Phys.*, 161(20), 204101.

Dinu, D.F., Tschöpe, M., Schröder, B., Liedl, K.R., Rauhut, G. (2022). Determination of spectroscopic constants from rovibrational configuration interaction calculations. *J. Chem. Phys.*, 157, 154107.

Duff, I.S., Grimes, R.G., Lewis, J.G. (1989). Sparse matrix test problems. *ACM Trans. Math. Softw.*, 15, 1–14.

Erfort, S., Tschöpe, M., Rauhut, G. (2020). Toward a fully automated calculation of rovibrational infrared intensities for semi-rigid polyatomic molecules. *J. Chem. Phys.*, 152, 244104.

Heislbetz, S. and Rauhut, G. (2010). Vibrational multiconfiguration self-consistent field theory: Implementation and test calculations. *J. Chem. Phys.*, 132(12), 124102.

Herman, M. and Perry, D.S. (2013). Molecular spectroscopy and dynamics: A polyad-based perspective. *Phys. Chem. Chem. Phys.*, 15, 9970–9993.

Hills, G.W., Foster, R.B., Jones, W.J. (1977). Raman spectra of asymmetric top molecules. *Mol. Phys.*, 33, 1571–1588.

Hougen, J., Bunker, P., Johns, J. (1970). The vibration-rotation problem in triatomic molecules allowing for a large-amplitude bending vibration. *J. Mol. Spectrosc.*, 34(1), 136–172.

Huron, B., Malrieu, J.P., Rancurel, P. (1973). Iterative perturbation calculations of ground and excited state energies from multiconfigurational zeroth-order wavefunctions. *J. Chem. Phys.*, 58(12), 5745–5759.

Kats, D. and Manby, F.R. (2013). Communication: The distinguishable cluster approximation. *J. Chem. Phys.*, 139(2), 021102.

Knizia, G., Adler, T.B., Werner, H.-J. (2009). Simplified CCSD(T)-F12 methods: Theory and benchmarks. *J. Chem. Phys.*, 130(5), 054104.

Koput, J. (2019). Ab initio structure and vibration-rotation dynamics of germylene, geh_2. *J. Comput. Chem.*, 40(21), 1911–1918.

Lai, S.-T. (1994). Computation of algebraic formulas for Wigner 3-j, 6-j, and 9-j symbols by maple. *Int. J. Quantum Chem.*, 52, 593–607.

Landau, L. and Lifshitz, E. (1977). *Quantum Mechanics*, 3rd edition. Pergamon Press, Oxford.

Langr, D. and Tvrdík, P. (2016). Evaluation criteria for sparse matrix storage formats. *IEEE Transactions on Parallel and Distributed Systems*, 27(2), 428–440.

Mant, B.P., Yachmenev, A., Tennyson, J., Yurchenko, S.N. (2018). ExoMol molecular line lists - XXVII. Spectra of C_2H_4. *Mon. Not. Royal Astron. Soc.*, 478(3), 3220–3232.

Mathea, T. and Rauhut, G. (2020). Assignment of vibrational states within configuration interaction calculations. *J. Chem. Phys.*, 152(19), 194112.

Mathea, T. and Rauhut, G. (2021). Advances in vibrational configuration interaction theory – part 1: Efficient calculation of vibrational angular momentum terms. *J. Comp. Chem.*, 42, 2321–2333.

Mathea, T., Petrenko, T., Rauhut, G. (2022). Advances in vibrational configuration interaction theory – part 2: Fast screening of the correlation space. *J. Comp. Chem.*, 43, 6–18.

Meisner, J., Hallmen, P.P., Kästner, J., Rauhut, G. (2019). Vibrational analysis of methyl cation-rare gas atom complexes: CH_3^+-Rg (Rg = He, Ne, Ar, Kr). *J. Chem. Phys.*, 150(8), 084306.

Messiah, A. (1962). *Quantum Mechanics*, volume 2. John Wiley and Sons Inc., New York.

Nikitin, A., Rey, M., Tyuterev, V. (2014). High order dipole moment surfaces of PH_3 and ab initio intensity predictions in the octad range. *J. Mol. Spectrosc.*, 305, 40–47.

Oschetzki, D. and Rauhut, G. (2014). Pushing the limits in accurate vibrational structure calculations: Anharmonic frequencies of lithium fluoride clusters $(LiF)_n$, n = 2-10. *Phys. Chem. Chem. Phys.*, 16, 16426–16435.

Owens, A., Yachmenev, A., Thiel, W., Tennyson, J., Yurchenko, S.N. (2017). Exomol line lists - xxii. The rotation-vibration spectrum of silane up to 1200K. *Mon. Not. Royal Astron. Soc.*, 471, 5025–5032.

Papousek, D. and Aliev, M.R. (1982). *Molecular Vibrational-Rotational Spectra*. Elsevier Scientific Publishing Company, Amsterdam.

Petrenko, T. and Rauhut, G. (2017). A new efficient method for the calculation of interior eigenpairs and its application to vibrational structure problems. *J. Chem. Phys.*, 146, 124101.

Pflüger, K., Paulus, M., Jagiella, S., Burkert, T., Rauhut, G. (2005). Multi-level vibrational SCF calculations and FTIR measurements on furazan. *Theor. Chem. Acc.*, 114, 327–332.

Podolsky, B. (1928). Quantum-mechanically correct form of Hamiltonian function for conservative systems. *Phys. Rev.*, 32, 812–816.

Puzzarini, C., Biczysko, M., Bloino, J., Barone, V. (2014). Accurate spectroscopic characterization of oxirane: A valuable route to its identification in Titan's atmosphere and the assignment of unidentified infrared bands. *Astrophys. J.*, 785(2), 107.

Rauhut, G. (2004). Efficient calculation of potential energy surfaces for the generation of vibrational wave functions. *J. Chem. Phys.*, 121(19), 9313–9322.

Rauhut, G., Knizia, G., Werner, H.-J. (2009). Accurate calculation of vibrational frequencies using explicitly correlated coupled-cluster theory. *J. Chem. Phys.*, 130(5), 054105.

Rey, M. (2022). Novel methodology for systematically constructing global effective models from *ab initio*-based surfaces: A new insight into high-resolution molecular spectra analysis. *J. Chem. Phys.*, 156, 224103.

Schneider, M. and Rauhut, G. (2024). VSCF/VCI theory based on the Podolsky Hamiltonian. *J. Chem. Phys.*, 160(21), 214118.

Schneider, M., Born, D., Kästner, J., Rauhut, G. (2023). Positioning of grid points for spanning potential energy surfaces - How much effort is really needed? *J. Chem. Phys.*, 158(14), 144118.

Schröder, B. (2023). Ab initio rovibrational spectroscopy of the acetylide anion. *Molecules*, 28, 5700.

Schröder, B. and Rauhut, G. (2022). Vibrational configuration interaction theory. In *Vibrational Dynamics of Molecules*, Bowman, J.M. (ed.). World Scientific Publishing, Singapore.

Schröder, B. and Rauhut, G. (2024). From the automated calculation of potential energy surfaces to accurate infrared spectra. *J. Phys. Chem. Lett.*, 15(11), 3159–3169.

Shore, B.W. and Menzel, D.H. (1968). *Principles of Atomic Spectra*. Wiley, New York.

Sparta, M., Høyvik, I.-M., Toffoli, D., Christiansen, O. (2009). Potential energy surfaces for vibrational structure calculations from a multiresolution adaptive density-guided approach: Implementation and test calculations. *J. Phys. Chem. A*, 113, 8712–8723.

Špirko, V., Jensen, P., Bunker, P., Čejchan, A. (1985). The development of a new Morse-oscillator based rotation-vibration Hamiltonian for H_3^+. *J. Mol. Spectrosc.*, 112(1), 183–202.

Strom, A.I., Muddasser, I., Rauhut, G., Anderson, D.T. (2024). Diborane anharmonic vibrational frequencies and intensities: Experiment and theory. *J. Mol. Spectrosc.*, 400, 111887.

Tschöpe, M. and Rauhut, G. (2022). Convergence of series expansions in rovibrational configuration interaction (RVCI) calculations. *J. Chem. Phys.*, 157(23), 234105.

Wang, S.C. (1929). On the asymmetrical top in quantum mechanics. *Phys. Rev.*, 34, 243–252.

Watson, J.K. (1968). Simplification of the molecular vibration-rotation Hamiltonian. *Mol. Phys.*, 15(5), 479–490.

Werner, H.-J., Knowles, P.J., Manby, F.R., Black, J.A., Doll, K., Heßelmann, A., Kats, D., Köhn, A., Korona, T., Kreplin, D.A. et al. (2020). The Molpro quantum chemistry package. *J. Chem. Phys.*, 152, 144107.

Yamada, K. (1983). Effect of phase choices in rovibrational wavefunctions on the labeling of k-and l-type doubling in molecular energy levels. *Zeitschrift für Naturforschung A*, 38(8), 821–834.

Yang, E.L., Spencer, R.J., Zhanserkeev, A.A., Talbot, J.J., Steele, R.P. (2023). Accelerating and stabilizing the convergence of vibrational self-consistent field calculations via the direct inversion of the iterative subspace (vDIIS) algorithm. *J. Chem. Phys.*, 159(8), 084103.

Yurchenko, S.N. (2023). *Computational Spectroscopy of Polyatomic Molecules*. CRC Press, Taylor & Francis Group, Boca Raton, FL.

Yurchenko, S.N., Carvajal, M., Jensen, P., Lin, H., Zheng, J., Thiel, W. (2005). Rotation-vibration motion of pyramidal XY_3 molecules described in the Eckart frame: Theory and application to NH_3. *Mol. Phys.*, 103, 359–378.

Yurchenko, S.N., Yachmenev, A., Ovsyannikov, R.I. (2017). Symmetry-adapted ro-vibrational basis functions for variational nuclear motion calculations: TROVE approach. *J. Chem. Theory Comput.*, 13, 4368–4381.

Yurchenko, S.N., Al-Refaie, A.F., Tennyson, J. (2018). EXOCROSS: A general program for generating spectra from molecular line lists. *Astron. Astrophys.*, 614(A131), 1–12.

Zare, R.N. (1988). *Angular Momentum: Understanding Spatial Aspects in Chemistry and Physics*. John Wiley & Sons, New York.

Ziegler, B. and Rauhut, G. (2016). Efficient generation of sum-of-products representations of high-dimensional potential energy surfaces based on multimode expansions. *J. Chem. Phys.*, 144(11), 114114.